耐火物成形体の圧密に伴う粒子充填構造変化の三次元解析

Three-dimensional analysis of particle packing structure change with compaction of refractory compacts

井形徹央*，松本成史**，髙見行平*

Tetsuo IGATA*, Shigefumi MATSUMOTO** and Kouhei TAKAMI*

1　緒言

一般的に耐火物の耐食性は気孔率と相関があることが知られており，耐食性の向上を図る上で成形体の充填密度をより高くすることは重要である。充填密度を向上させる手法として Furnas [1] や Andreasen ら [2] の連続粒度分布式といった最密充填構造を狙った粒度構成とすることが挙げられる。しかし現実には充填時の偏析や粒子間相互作用により均質な充填構造を得ることは難しいほか，成形後の充填構造が狙い通りの最密充填構造にならないと考えられる。そのため，成形体の充填密度とその内部構造の関係性を明らかにする事は耐火物の耐食性向上を図る上で重要である。

耐火物の内部構造を評価する方法として X 線 CT（X-ray computed tomography）を活用し，三次元的に内部構造を観察する方法がある。X 線 CT の耐火物への応用例としては非破壊欠陥探査装置としての活用 [3] のほか，多孔体の気孔構造解析 [4] が報告されている。

本研究では X 線 CT により耐火物成形体内の粗粒を可視化できる事に着目し，成形圧を変化させたときの粗粒充填構造の可視化を行い，その構造の評価を行った。

2　実験方法

2・1　試験サンプル

本報告では模擬的な MgO- 黒鉛系を使用して評価を行う。MgO 原料は破砕粒子で比較的長く角ばった不規則形状を有する平均粒径 2.0mm の粗粒，そして平均粒径 0.21mm の微粒の 2 種類を用い，黒鉛も同様の不規則形状粒子で平均粒径は 0.25mm であった。各原料を**表 1** に示す 60:25:15 の配合割合で有機

1 Introduction

Generally, it is known that the refractories corrosion resistance is correlated with the porosity, so to improve the corrosion resistance, it is important to make packing density of the compact higher. As a technique to improve packing density, the grain size distribution composition aiming at the close-packed structure such as Furnas[1], Andreasen and Andersen[2] continuous grain size formula can be mentioned. However, in reality, it is difficult to obtain a homogeneous packing structure due to segregation and interparticle interaction during packing, and it is considered that the packing structure after molding does not become the desired close-packed structure. Therefore, it is important to clarify the relationship between packing density of the compact and the internal structure in order to improve refractories's corrosion resistance.

As a method for evaluating the internal structure of refractories, there is a method for three-dimensionally observing the internal structure by utilizing X-ray CT (X-ray computed tomography). As application examples of X-ray CT to refractories, utilization as a nondestructive defect exploration[3] and pore structure analysis of porous materials[4] are reported.

In this study, from the viewpoint of visualization of coarse grains in refractories compacts by X-ray CT, visualization of coarse grain filling structure was carried out when compacting pressure was changed, and the structure was evaluated.

2 Experiments

2・1 Preparation of test pieces

In this report, the evaluation is carried out using a simulated MgO- graphite system. Table 1 shows the blending ratio. MgO raw materials used are mean particlesize 2.0 mm coarse particles which are crushed particles and have relatively long and angular irregular shapes, and mean particlesize 0.21 mm fine particles. 2 kinds of MgO raw materials are used. From mixture, where each raw material was mixing with an organic binder at a blending ratio of 60: 25: 15 as shown in **Table 1**, 5 samples of A to E were obtained, which were compacted

＊　技術研究所 製品プロセス研究センター　Product R&D Center, Technical Research Labs.
＊＊ 技術研究所 共通基盤研究センター アシスタントマネージャー　Assistant Manager, Fundamental Technology Research Center, Technical Research Labs.

Table 1 Composition and forming conditions of the prepared samples.

Sample		A	B	C	D	E
Composition		/ Volume%				
Aggregate	MgO Coarse grain (2.0*)	60				
Matrix	MgO Fine grain (0.21*)	25				
	C (Graphite) (0.25*)	15				
Forming condition						
Compaction pressure, *P* / MPa		3	20	50	125	215
Pressurized area / mm × mm		160 × 40			230 × 100	

*grain size / mm

バインダーと共に混練した坏土から**表 1** に示す 3 ～ 215MPa の各圧力で成形した A ～ E の 5 種類のサンプルを得た。また ,サンプル A ～ C の成形体からそれぞれ 40 × 40 × 40mm の角柱状，そしてϕ 30 × 40mm の円柱状試験片を切り出し，X 線 CT による三次元内部構造観察による解析に供した。なお，ここでは成形体中の MgO 粗粒を「骨材」として，それ以外の部分，つまり MgO 微粒と黒鉛および空気が混在している部分を「マトリクス」と称する。また , 観察用サンプルとは別に同一配合割合の混練坏土を用いた一軸圧縮試験機によってϕ 60mm の金型中で最大 120MPa まで加圧し, 圧密過程の連続的測定も行った。

２・２　X 線 CT を用いた 3 次元内部構造観察

各サンプルについて X 線 CT による断層画像の撮像を行った。**図 1** に X 線 CT の概念図を示す。三次元的に内部構造を観察するためには，被検体に対して様々な方向から透視画像を撮影する必要があり，医療用装置では患者を中心として対角に配置された X 線源と X 線検出装置が患者の周りを回転しながら撮影する。これに対してここで用いる産業用 X 線 CT 装置では X 線源と検出器を固定し，被検体を回転させながら撮影する。X 線は物体を透過する際に吸収され減衰する。この透過 X 線の強度分布を二次元投影像として被検体半周分だけ測定し，各水平断面を画像再構成することにより数百から数千枚の二次元断層を取得できる。再構成した断層像の各ピクセルの輝度は X 線が透過する際に対象物にどれだけ吸収され

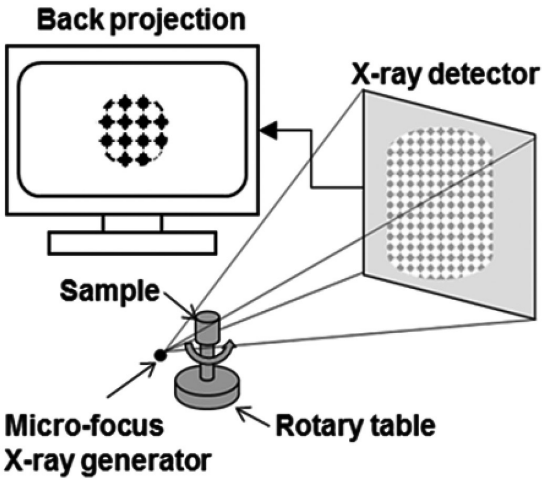

Fig. 1 Schematic image of 3 dimensional X-ray CT.

at each pressure of 3 ~ 215 MPa as shown in **Table 1**. Prismatic and cylindrical specimens of 40 * 40 * 40 mm and 30 * 40 mm diameter, respectively, were cut out from the compacts of samples A to C and analyzed by X-ray CT to observe the three-dimensional internal structure. Here, coarse MgO grains in the compact are referred to as "aggregate", and the other parts, that is, the parts where fine MgO grains, graphite, and voids coexist, are referred to as "matrix". And, apart from the sample for observation, a uniaxial compression testing machine using mixing mixture of the same mixing ratio was used to pressurize up to 120 MPa in a die of ϕ60mm, and continuous measurement of consolidation process was also carried out.

2・2 Observation of three-dimensional internal structure using X-ray CT

Tomographic imaging by X-ray CT was carried out

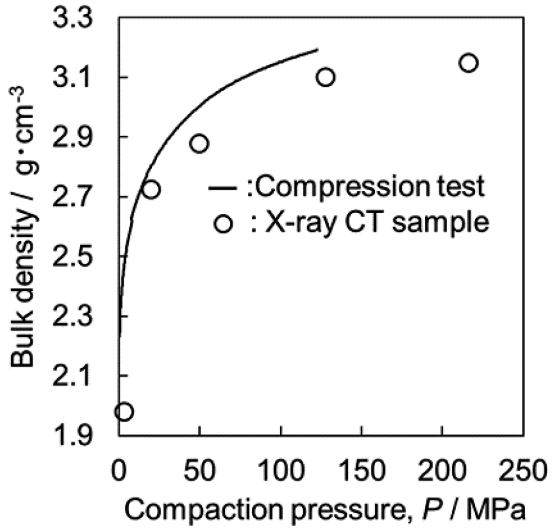

Fig. 2 Compaction pressure vs. bulk density.

たかに影響され，X 線が透過しやすい物質は輝度が低く（暗く），透過しにくい物質は高く（明るく）表示されるため，測定対象物内部の構成物質を識別することが可能となる。

本試験で得られた断層画像はそのままではノイズにより骨材とそれ以外の部分の境界が不明瞭であるため，画像処理ソフトウェアを用いて輝度の閾値を決定し，二値化処理を行うことで骨材のみを分離した断層画像を得た。また，得られた二値化画像を Z 方向に積層することで骨材の三次元充填構造を再現した。

3　結果

3・1　坏土の圧縮特性

図 2 に X 線 CT 観察を行った各サンプルのかさ密度測定結果および一軸圧縮試験機によって測定した成形圧とかさ密度の関係を示す。ただし，サンプル A のかさ密度は測定中に表面が崩壊したため正確な値が測定できていない。また**表 2** に観察試料のかさ密度と見かけ気孔率を示す。

3・2　X 線 CT から得られた断層画像

図 3(a) ～ (e) に各サンプルの中心付近を 15mm 四方にトリミングした断層画像の例を示す。また，**図 3** 下に各サンプルから得られた断層画像の枚数と 1 ピクセルの 1 辺の長さを示す。X 線 CT からは**図 3** に示すような断層画像が**図 3** 下表に示した枚数分得られる。これらの断層画像の間隔は 1 ピクセルの辺の長さに等しい。画像中の輝度の違いはその場所にある物

Table 2 Density and porosity data of samples. (*Sample broken during test.)

Sample	A	B	C	D	E
Bulk density / g·cm^{-3}	2.3*	2.78	2.91	3.10	3.14
Apparent porosity / %	30*	15.3	11.3	4.7	3.0

for each sample. **Fig. 1** shows a conceptual image of X-ray CT. In order to observe the internal structure three-dimensionally, it is necessary to photograph the fluoroscopic image for the subject from various directions, and in the medical equipment, it is photographed, while X-ray source and X-ray detector which are arranged in the diagonal as a center of the patient rotate around the patient. On the other hand, in the industrial X-ray CT equipment used here, the X-ray source and the detector are fixed, and the subject is photographed while rotating. X-rays are absorbed and attenuated as they pass through an object. The intensity distribution of this transmitted X-ray is measured as a 2-dimensional projection image by the half circumference of the subject, and several hundred to several thousand sheets of 2-dimensional fault can be acquired by image reconstruction of each horizontal cross section. Since the luminance of each pixel of the reconstructed tomographic image is affected by how much the X-ray is absorbed by the object when it is transmitted, and the material which is easy to transmit the X-ray has low luminance (dark), and the material which is difficult to transmit the X-ray has high luminance (bright), it becomes possible to discriminate the constituent material in the measurement object.

Since the boundary between the aggregate and the other part is indistinct by the noise in the tomographic image obtained in this test as it is, the threshold of the luminance was decided using the image processing software, and the tomographic image in which only the aggregate was separated was obtained by carrying out the binarization processing. And, the three-dimensional filling structure of the aggregate was reproduced by laminating got binary image in the Z direction.

3 Experimental result

3・1 Mmixture compression characteristics

Fig. 2 shows the results of bulk density measurement and the relationship between compaction pressure and bulk density measured by a uniaxial compression tester for each sample subjected to X-ray CT observation. However, the exact value of the bulk density of sample A cannot be measured because the surface collapsed during measurement. **Table 2** shows the observed bulk density and apparent porosity.

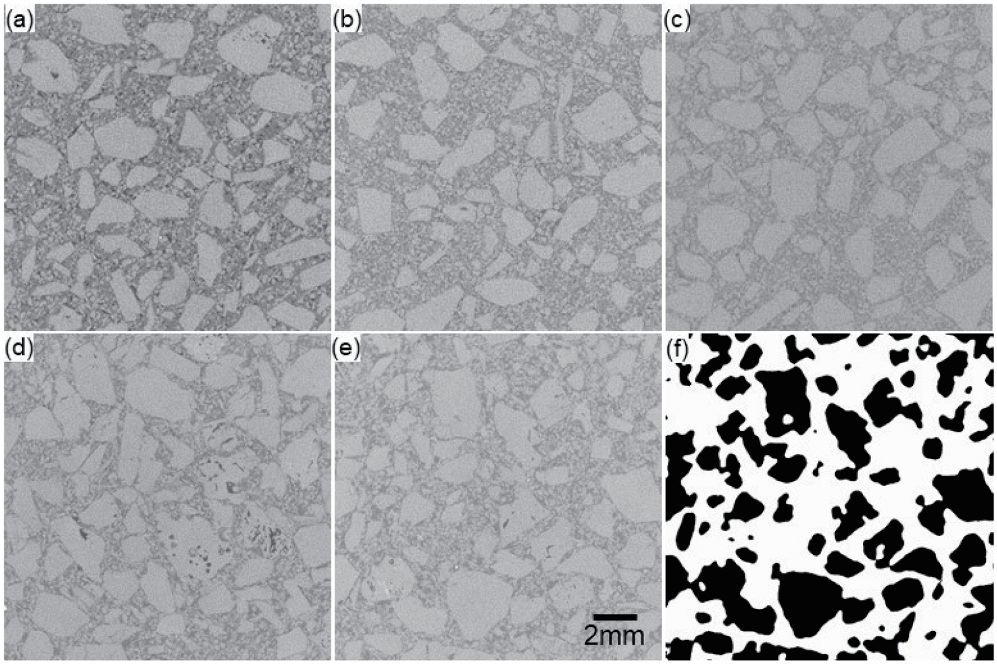

Sample	A	B	C	D	E
No. of pictures	1212 ~1304	1212 ~1291	1212 ~1264	1667 ~2000	1622 ~2000
Pixel size / mm・pixel^{-1}	0.033 ~0.028	0.033 ~0.030	0.033 ~0.030	0.023 ~0.019	0.026 ~0.019

Fig. 3 2D-CT images from sample A~E are shown in (a)~(e), respectively, and representative binarized image for sample E in (f).

質に影響され，本試験で用いたサンプルでは黒く見える部分が空気，灰色に見える部分が黒鉛，白く見える部分が MgO 粒子と対応する。この様に断層画像では角ばった骨材が組織中に分布している様子を確認できた。また，骨材の一部は内部に空隙を持っていることが確認できた。**図 3(f)** に**図 3(e)** の二値化処理後の断層画像を示す。この方法で白色部分のマトリクス中に黒色部分とし骨材が抽出できていることが確認できた。同様の処理を施した連続断層画像を Z 方向に積層することで抽出した部分の三次元構造を再構成した。

３・３　再構成された粒子充填構造解析結果

図 4 に関心領域中で再構成された各サンプルの三次元の粒子充填構造を示す。画像の関心領域の一辺は 15mm の立方体であり，領域の境界を跨ぐ粒子は表示していない。各サンプルとも骨材の粒子充填構造を可視化できている事が確認できた。各サンプルの再構成画像を見ると成形圧が非常に小さいサンプル

3・2 Tomographic images obtained from X-ray CT

Figure 3(a)~(e) shows an example of a tomographic image obtained by trimming the vicinity of the center of each sample to 15 mm squares. And, the number of tomographic images obtained from each sample and the length of one side of one pixel are shown at the bottom of **Fig. 3**. From X-ray CT, tomographic images as shown in **Fig. 3** are obtained by the number of sheets shown in the lower part of **Fig. 3**. The distance between these tomographic images is equal to the length of the side of one pixel. The difference of the luminance in the image is affected by the material in the place, and in the sample used in this test, the black part corresponds to the air, the gray part corresponds to the graphite, and the white part corresponds to the MgO particle. In the tomographic image, the state in which the angular aggregate was distributed in the tissue was able to be confirmed. And, it was confirmed that the part of the aggregate had the void in the inside. **Figure 3(f)** shows a tomographic image of the **Fig. 3(e)** after binarization processing. It was confirmed that black part and phalanges were able to be extracted in the matrix of the white part by this method. The three-dimensional structure of the extracted part was reconstructed by laminating the continuous tomographic

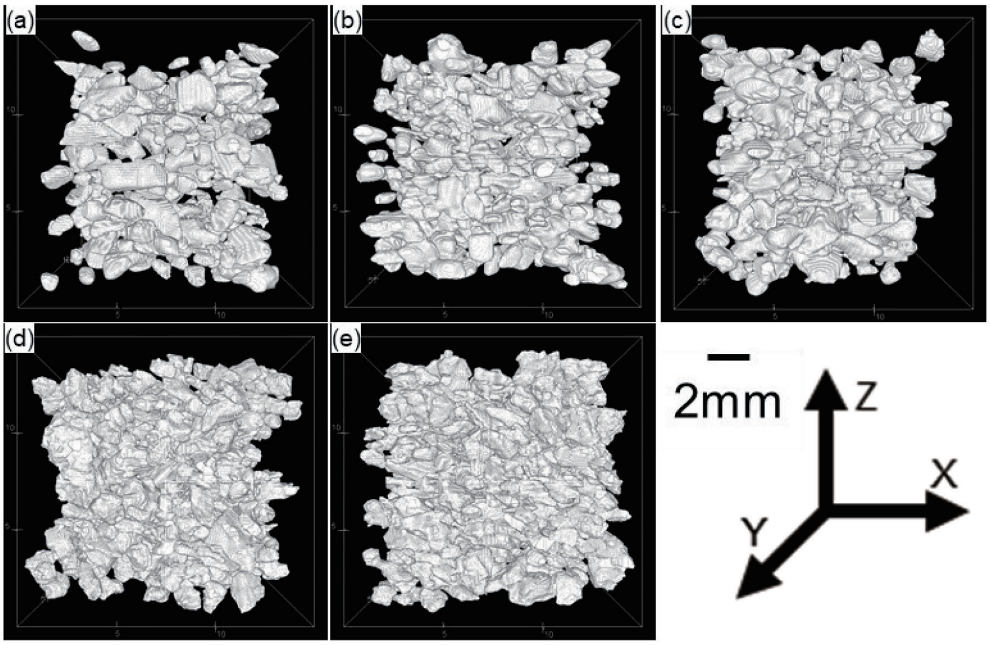

Fig. 4 3D-CT images for the sample A~E shown in (a)~(e).

A から成形圧が高まるにつれて骨材同士が接近し，より密に充填されている様子が観察できた。またサンプル B ではサンプル A に比べ一部のアスペクト比の大きい粒子が成形方向に対して直角方向に配向していることが確認できた。

これらの再構成された充填構造の解析を行った。画像解析ソフト上で再構成された各粒子を識別し，関心領域内の粒子の個数とそれぞれの粒子の体積を解析した。解析結果を**表 3** に示す。成形圧が高いサンプルほどの関心領域中の骨材の体積割合および粒子

Table 3 Particle analysis result of the volume fraction and number of grains.

	A	B	C	D	E
Volume fraction / %	27.5	33.5	41.3	49.4	44.8
Number of grain in region of interest / $15^3 mm^3$	214	266	223	429	426

Table 4 Mean and mode inter-particle distance.

	A	B	C	D	E
Mean distance / mm	1.66	1.28	1.17	0.75	0.85
Mode distance / mm	1.35	1.14	1.23	0.63	0.72
Standard deviation	0.77	0.48	0.43	0.28	0.34

image with the similar processing in the Z direction.

3・3 Reconstructed particle-filled structure analysis results

Fig. 3 shows a three-dimensional particle packing structure of each sample reconstructed in the region of interest. One side of the region of interest in the image is a 15 mm cube, and particles crossing the boundary of the region are not displayed. It was confirmed that the particle filling structure of the aggregate could be visualized in each sample. In the reconstructed image of each sample, it was observed that the aggregates approached each other and filled more closely as the forming pressure increased

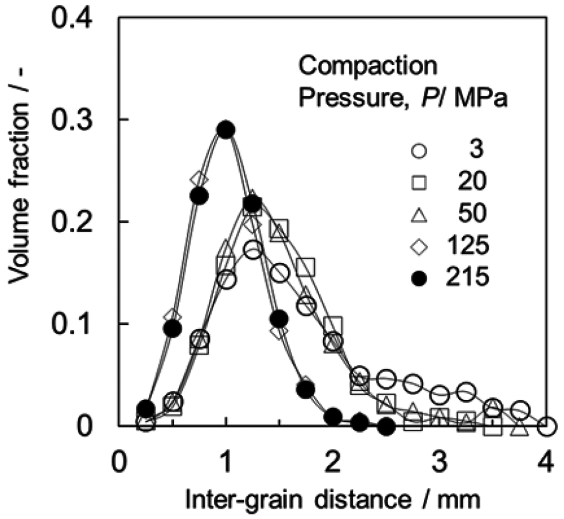

Fig. 5 Effect of compaction pressure on the inter-grain distance distribution in the compact.

数が大きくなっている傾向が確認できた。また，成形体中のマトリクスにある各点からいずれかの骨材表面までの最短距離を解析する手法を用いて，骨材の粒子間隔の解析を行った。この解析を行うことで骨材の充填構造を間接的に測定することができる。粒子間隔の分布を**図 5** と**表 4** に示す。成形圧が高いほど骨材間の隙間が狭くなることが分かる。また特にサンプル A と B，サンプル C と D でそれぞれ分布が変化し，125MPa 以上ではほぼ変化が無いことが確認された。

4　考察

X 線 CT 観察により確認された成形圧ごとの粒子充填構造と一軸成形に伴うかさ密度変化の関係について考察する。Cooper ら [5] は，粉体層の圧縮はそれを構成する各粉末の粒子の再配列と粒子の塑性変形の二つの過程により起こるという考えに基づき，粉体層の圧縮挙動を詳細に説明できる以下の関係式を提唱している。

$$\frac{V_0 - V}{V_0 - V_\infty} = a_1 \cdot \exp\left(-\frac{k_1}{P}\right) + a_2 \cdot \exp\left(-\frac{k_2}{P}\right) \quad (1)$$

ここで，V0: 圧縮圧力 P=0 のときの粉体かさ体積，V ∞ : 粉体の正味体積，V: 圧縮圧力が P のときの粉体体積である。この式の左辺は，圧縮前の粉体層の全空隙体積に対する圧縮圧力 P で消滅した空隙体積の割合を示し，体積圧縮率と呼ばれる。右辺は第 1 項が粒子再配列，第 2 項が粒子の塑性変形に関係しており，a_1 及び a_2 はそれぞれの圧縮機構における最大体積圧縮率，k_1, k_2 はそれぞれの圧縮機構が開始する圧力を示している。したがって k_1 および k_2 の値を求めることにより，成形時の粉体の圧縮挙動を推測できる。**図 6** に**図 2** に示した一軸圧縮試験の結果から計算した体積圧縮率と圧力の関係および Cooper の式で近似した曲線および近似計算により得られた係数 a 及び k の値を示す。図中の実線が実測値，破線が近似値である。**図 6** に示した実測値と近似値はよく一致しており，本試験で測定した系の圧縮挙動は Cooper の考えた二つの過程に分けられると考えられる。つまり，粒子の移動を伴う圧縮は**図 6** に示すように k_2 = 30.5MPa より低い圧力までで完了し，それ以降は粒子の塑性変形が起こると推測できる。

先述の圧密挙動による推測と X 線 CT による粒子

from the sample A in which the forming pressure was very small. In sample B, it was confirmed that some particles with larger aspect ratio were oriented in the direction perpendicular to the forming direction than in Sample A.

These reconstructed filling structures were analyzed. Each particle reconstructed on the image analysis software was distinguished, and number of particles in the region of interest and volume of each particle were analyzed. The analysis results are shown in **Table 3**. It was confirmed that the higher the compaction pressure, the larger the volume fraction of aggregate and the larger the number of particles in the region of interest. And, the particle interval of the aggregate was analyzed using the technique which analyzed the shortest distance from each point in the matrix in the compact to either aggregate surface. By carrying out this analysis, it is possible to indirectly measure the filling structure of aggregate. The distribution of particle spacing is shown in **Fig. 5** and **Table 4**. It can be seen that the higher the molding pressure, the narrower the gap between aggregates. Especially, it was confirmed that the distribution changed in samples A and B and samples C and D respectively, and that there was almost no change over 125 MPa.

4 Discussion

The relationship between the particle packing structure at each molding pressure and the density change with uniaxial molding confirmed by X-ray CT observation is examined. Cooper and Eaton[5] proposed the following relational equation which can explain the compression behavior of powder layer in detail, based on the idea that the compression of powder layer is generated by two processes of rearrangement of particles of each powder which constitutes it and plastic deformation of particles.

$$\frac{V_0 - V}{V_0 - V_\infty} = a_1 \cdot \exp\left(-\frac{k_1}{P}\right) + a_2 \cdot \exp\left(-\frac{k_2}{P}\right) \quad (1)$$

where V0 is the bulk volume of the powder when the compressive pressure P = 0, V ∞ is the net volume of the powder, and V is the volume of the powder when the compressive pressure P. The left side of the equation represents the ratio of the volume of voids dissolved at the compression pressure P to the total volume of voids in the powder layer before compression, which is called the volume compressibility. On the right side, the 1st term is related to particle rearrangement and the 2nd term is related to particle plastic deformation, and α_1 and α_2 show the maximum volume compressibility in each compression mechanism, and k_1 and k_2 show the pressure at which each compression mechanism starts. Therefore, by obtaining the value of k_1 and k_2, the compression behavior of the powder in forming can be estimated. **Fig. 6** shows the relationship between volume compressibility and pressure calculated from the results of the uniaxial compression test

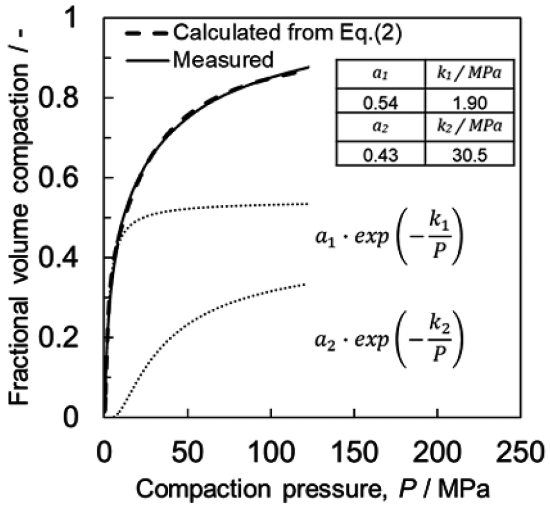

Fig. 6 Fractional volume compaction vs pressure.

充填構造解析結果を比較する。X 線 CT で観察された骨材充填構造の変化は**表 3** と**表 4** および**図 5** に示すとおりサンプル A, B 間(3 ～ 20MPa）とサンプル C, D 間（50 ～ 125MPa）確認された。サンプル A から B にかけては粗粒より大きな空隙が消失しており，この間で粒子は大きく移動して充填に近い状態へ粒子が再配列されたことが分かる。サンプル C，D 間では更に空隙が狭くなっていっていることに加え，粒子数が明確に増加した。つまり骨材は 50 ～ 125MPa の間でもマトリクスを押しのけて移動しており，Cooper の式による近似で得られた推測と異なる結果となる。これは骨材の移動に伴うマトリクスの変形が見かけ上大きな粒子の塑性変形として振舞うためであると考えられる。**図 7** にモデル図を示す。粒度分布を持つ坏土を充填すると巨視的，微視的問わず不均一な充填構造となり，局所的に微粒が集合した部分が現れる。成形圧がまだ低いうちは粒子間の空隙を排除して再配列が行われるが，ある程度充填が進むと骨材の移動先（**図 7(B)** 破線の位置）に既に微粒の塊が充填された状態が現れる。1 つの固体である骨材に比べ微粒の塊は軟らかく変形することが可能である。つまり，この微粒の塊の流動が見かけ上粒子の変形として圧縮試験では捉えられたのだと考えられる。

5　まとめ

成形圧の異なるれんがに対して X 線 CT を用いた粒子充填構造の三次元観察を行い坏土の圧縮特性と比較した結果，以下のことがわかった。

shown in **Fig. 2** and the curve approximated by Cooper's equation. The solid line in the **Fig. 6** is the measured value, and the broken line is the approximate value. **Fig. 6** shows the values of the coefficients obtained by the approximate calculation. The compression behavior of the system measured in this test is considered to be divided into two processes considered by Cooper. That is, as shown in **Fig. 6**, compression with particle migration is completed at pressures lower than k_2 = 30.5 MPa, after which it can be assumed that particle plastic deformation occurs.

The results of particle packing structure analysis by X-ray CT are compared with those estimated by the above consolidation behavior. As shown in **Tables 3, 4**, and **Fig. 5**, changes in the aggregate filling structure observed on X-ray CT were confirmed between Samples A and B (3 ~ 20 MPa) and between Samples C and D (50 ~ 125 MPa). The voids larger than the coarse particles disappeared from Sample A to Sample B, indicating that the particles were largely moved and rearranged to a state close to packing during this period. In addition to the narrower voids between samples C and D, the number of particles clearly increased. That is to say, the aggregate moves by pushing the matrix even between 50 ~ 125 MPa, and the result is different from the estimation obtained by the approximation by Cooper's equation. It is considered that this is because the deformation of the matrix with the transfer of the MgO coarse grain behaves as plastic deformation of the apparently large grain. A model diagram is shown in **Fig. 7**. When mixture with a large grain size distribution are filled, a nonuniform filling structure appears irrespective of macroscopic or microscopic observation, and a part where fine particles locally gather appears. While the forming pressure is still low, the voids between particles are removed and the rearrangement is carried out, and when the filling advances to some extent, the state in which the granular lump has already been filled in the moving destination (**Fig. 7 (B)** Dashed Line Locations) of the MgO coarse grain appears. It is possible that the lump of the fine grain is softly deformed in comparison with the MgO coarse grain which is one solid. That is to say, the flow of this fine particle lump seems to be caught as deformation of the particle in the compression test. Since the deformation pressure of this granular mass is much weaker than that of plastic deformation of MgO, it can be explained that the value obtained in this study is smaller than that obtained when MgO itself is compressed.

5 Conclusion

The three-dimensional observation of the particle-filling structure using X-ray CT was carried out for bricks with different molding pressures, and the results were compared with the compression characteristics of mixture.

・It is possible to visualize the internal structure of the compacts using X-ray CT.

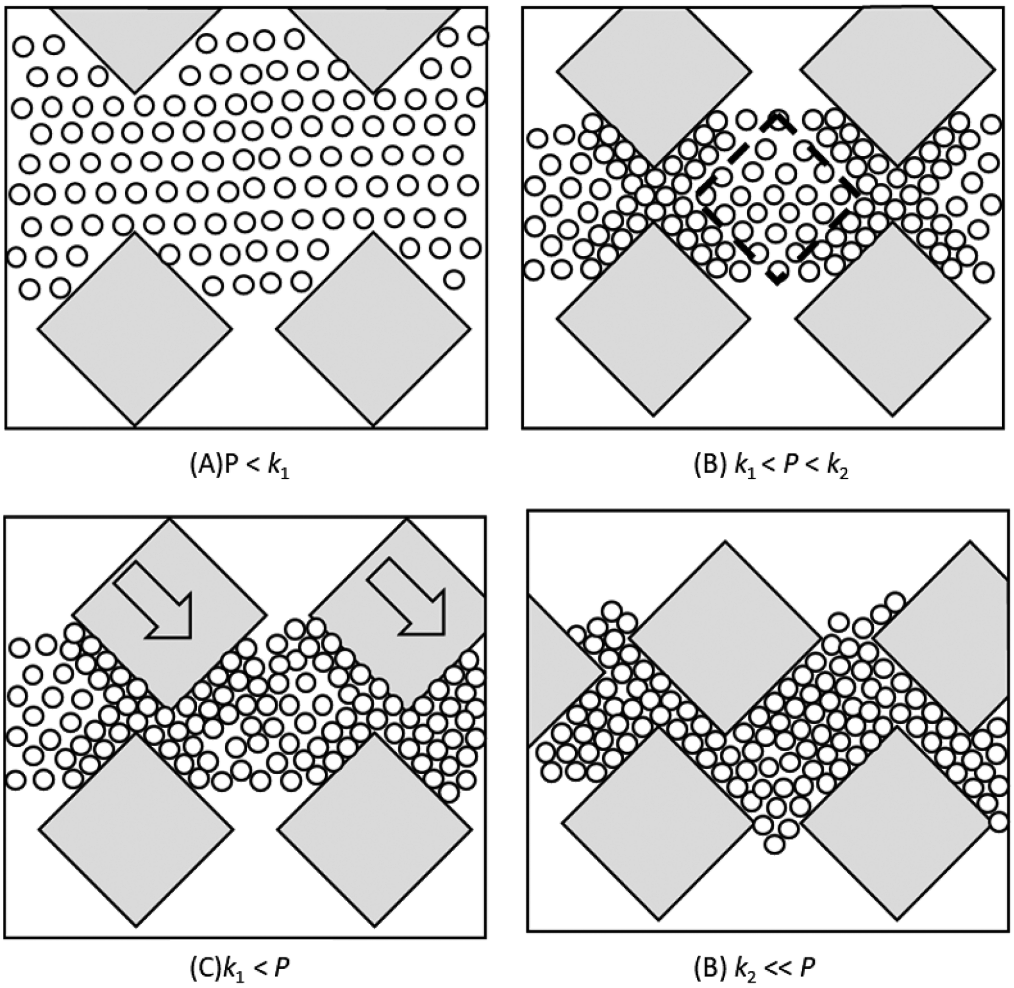

Fig. 7 Schematic image of particle packing with matrix deformation.

・X 線 CT を用いてれんがの内部構造を可視化することが可能である。

・適切な画像処理を行うことにより MgO 粗粒の充填構造を三次元的に評価することが可能となる。

・圧密に伴う MgO 粗粒の充填構造の変化は圧縮試験と Cooper の式による近似から得られる推測と異なる挙動を示した。

・骨材の再配列は Cooper の式による近似から推測される活性化圧力 k_2 より高圧でも進行することを確認した。この違いは k_2 より高圧ではマトリクスの流動，変形が起こることで見かけ上粒子の塑性変形として振舞うことが原因と推測された。

・By carrying out the appropriate image processing, it becomes possible to evaluate three-dimensional filling structure of the MgO coarse grain.

・The change of packing structure of MgO coarse grains with consolidation showed different behavior from the estimation obtained from the compression test and the approximation by Cooper's equation.

・It was confirmed that the rearrangement of aggregate proceeded even at higher pressure than the activation pressure k_2 estimated from the approximation by Cooper's equation. This difference was supposed to be caused by the flow and deformation of the matrix at higher pressure than k_2, which apparently acted as plastic deformation of the particles.

文　献

1）C.C. Furnas: U. S. Bur. Mines, Rept. Invest., 1928, No.2894, 7 (1928).

2）A. H. M. Andreasen and J. Andersen: Kolloid-

Reference

1) C.C. Furnas: U. S. Bur. Mines, Rept. Invest., 1928, No.2894, 7 (1928).

2) A. H. M. Andreasen and J. Andreasen: Kolloid-Zite., **50**, 217-228 (1930).

3) Y. Aiba et al.: Tetsu-to-Hagane (J. Iron and Steel Int. Japan), **14** [71] 1692-1699 (1985).

Zite., 50, 217-228 (1930).
3) 相庭吉郎他：鉄と鋼 **71** [14] 1692-1699 (1985).
4) 山田啓介他：第 6 回鉄鋼用耐火物専門委員会講演会報告集，耐火物技術協会 (2018) pp.75-82.
5) A. R. Cooper Jr and L. E. Eaton: J. Am. Ceram. Soc., **45** [3] 97-101 (1962).

本論文は以下の報文を翻訳・加筆・再構成して転載したものである。
井形他：第 7 回鉄鋼用耐火物専門委員会講演会報告集 (2019) pp.192-199.

4) K. Yamada et al.: (Proc.) Proceeding of the Sixth Meeting for Special Committeee on Refractries for Iron and Steel, TARJ, (2018) pp.75-82.
5) A. R. Cooper Jr and L. E. Eaton: J. Am. Ceram. Soc., **45** [3] 97-101 (1962).

This paper is translated and reprinted with some additions and reconstructions to the following paper:
Tetsuo Igata et al.: Proceedings of the 7th Annual Meeting of Technical Committee on Refractories for Iron and Steel, Technical Association of Refractories, Japan (2019) pp.192-199.